

# Vessel-Promoted OCT to OCTA Image Translation by Heuristic Contextual Constraints

Shuhan Li, Dong Zhang, Xiaomeng Li, Chubin Ou, Lin An, Yanwu Xu, Kwang-Ting Cheng, *Fellow, IEEE*

**Abstract**—Optical Coherence Tomography Angiography (OCTA) has become increasingly vital in the clinical screening of fundus diseases due to its ability to capture accurate 3D imaging of blood vessels in a non-contact scanning manner. However, the acquisition of OCTA images remains challenging due to the requirement of exclusive sensors and expensive devices. In this paper, we propose a novel framework, TransPro, that translates 3D Optical Coherence Tomography (OCT) images into exclusive 3D OCTA images using an image translation pattern. Our main objective is to address two issues in existing image translation baselines, namely, *the aimlessness in the translation process* and *incompleteness of the translated object*. The former refers to the overall quality of the translated OCTA images being satisfactory, but the retinal vascular quality being low. The latter refers to incomplete objects in translated OCTA images due to the lack of global contexts. TransPro merges a 2D retinal vascular segmentation model and a 2D OCTA image translation model into a 3D image translation baseline for the 2D projection map projected by the translated OCTA images. The 2D retinal vascular segmentation model can improve attention to the retinal vascular, while the 2D OCTA image translation model introduces beneficial heuristic contextual information. Extensive experimental results on two challenging datasets demonstrate that TransPro can consistently outperform existing approaches with minimal computational overhead during training and none during testing. The code is available at: [TransPro](#).

**Index Terms**—Image translation, OCT and OCTA images, Model promotion, Contextual constraints.

## I. INTRODUCTION

Ophthalmologists utilize Optical Coherence Tomography (OCT) and OCT Angiography (OCTA) as important imaging technologies for diagnosing retina diseases [1]–[3]. OCT is a non-invasive imaging modality that provides 3D cross-sectional visualization of the retina, which is critical for diagnosing various eye diseases, including aged-related macular degeneration, diabetic retinopathy, and glaucoma [4]. However, OCT has limitations in visualizing blood flow information, such as vessel density, as it is only capable of visualizing the retinal vessel structures [3], [5]. To address this limitation, OCTA was developed as an extension of OCT to provide clear

visualization of the retinal capillary networks [6]. In clinical practice, the OCTA device performs repeated scans of the OCT cross-sectional images at the same location, enabling detection of dynamic signals produced by moving red blood cells [7]. With the availability of OCTA images, early detection of some eye diseases, such as choroidal neovascularization for wet aged-related macular degeneration, has become possible.

Despite the usefulness of OCTA images, their clinical application is hindered by two major limitations [3], [8], [9]. Firstly, the cost of OCTA devices is a significant drawback, which poses a financial burden on both healthcare institutions and patients. The high cost is mainly attributed to the additional hardware and software required to capture and process OCTA images [8]. Secondly, OCTA suffers from the unstable image quality, which is caused by prolonged scanning time required for image acquisition. This longer scanning time can lead to involuntary eye movements and motion artifacts that can negatively affect the quality of OCTA images [9].

To address limitations of OCTA imaging limitations, the generation of OCTA images from OCT images has been proposed as a promising solution. Several studies have put forth different approaches [10]–[12], typically utilizing a UNet [13] as the backbone and adopting a generative-adversarial learning framework for pixel-to-pixel image translation [14], [15]. However, the quality of the translated OCTA images is usually sub-optimal, particularly in depicting fine retinal vascular areas that are typically ambiguous and unfaithful. Some recent methods have incorporated additional information, such as texture features [11] or adjacent slices [12], to improve the quality of the translated OCTA images. Despite these efforts, the results are still unsatisfactory. Therefore, further advancements are necessary to enhance the translation accuracy of OCTA images, to meet the clinical application requirements.

As illustrated in Figure 1, this paper presents an exploration on shortcomings of existing baseline models for OCT image to OCTA image translation, and aims to address these issues with two proposed modules.

**Problem-1: aimlessness in the translation process.** The current translation models are trained using an overall computational loss function, which fails to distinguish between vascular and non-vascular areas during the learning process [16]. As a result, the model prioritizes minimizing the loss, causing poor quality in the thin vascular areas which are crucial in clinical applications. To illustrate this problem, the translated OCTA image of an input OCT image in Figure 1 (a) exhibits a pixel ambiguity issue in the vascular areas, as seen in Figure 1 (b). However, our proposed Vessel Promoted Guidance (VPG) module (Figure 1 (c)) can resolve this problem.

S. Li and D. Zhang are with Department of Computer Science and Engineering, The Hong Kong University of Science and Technology, Hong Kong, China. E-mail: [slidm@connect.ust.hk](mailto:slidm@connect.ust.hk); [dongz@ust.hk](mailto:dongz@ust.hk).

C. Ou is with Weizhi Meditech (Foshan) Co., Ltd, China. E-mail: [cou@connect.ust.hk](mailto:cou@connect.ust.hk).

L. An is with Guangdong Weiren Meditech Co., Ltd, China. E-mail: [wqinjinia@weirenmeditech.com](mailto:wqinjinia@weirenmeditech.com).

Y. Xu is with South China University of Technology, and Pazhou Lab, China. E-mail: [ywxu@ieec.org](mailto:ywxu@ieec.org).

X. Li and K. Cheng are with Department of Electronic and Computer Engineering, The Hong Kong University of Science and Technology, Hong Kong, China. E-mail: [{eexmli, timcheng}@ust.hk">{eexmli, timcheng}@ust.hk](mailto).

Corresponding author: Xiaomeng Li.

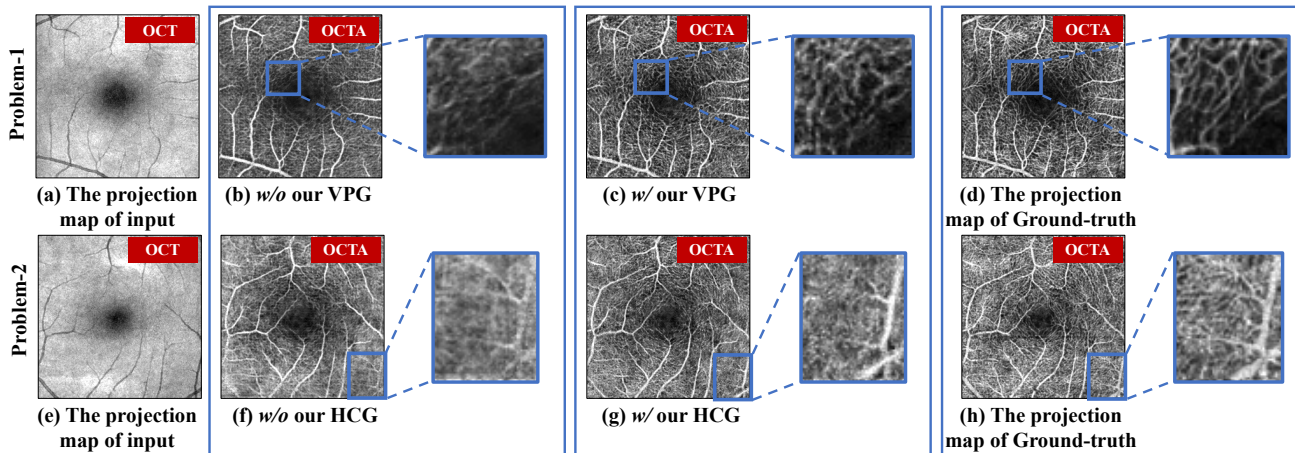


Fig. 1: There are two potential problems in the existing OCT to OCTA image translation baselines: (Problem-1) *aimlessness in the translation process*, and (Problem-2) *incompleteness of the translated object*. By Problem-1, we mean that although the overall quality of the obtained OCTA is satisfactory, quality of the retinal vascular (which are important in clinical practice) is not significantly improved. By Problem-2, we mean that the translated objects (e.g., retinal vascular and background regions) in OCTA has incompleteness due to the lack of global contextual information in the translation process. Our proposed Vessel Promoted Guidance (VPG) module and Heuristic Contextual Guidance (HCG) module can address these problems, where “w/o” and “w/” denote “without” and “with”, respectively. The blue frames highlight the improved areas predicted by TransPro.

**Problem-2: incompleteness of the translated object.** Insufficient contextual information is a common issue in pixel-level computer vision tasks, which results in incomplete object localization or separation [17], [18]. Similarly, in OCT to OCTA image translation, the lack of visual contexts may lead to discontinuities in the vascular areas [19]. For example, the OCTA image of an input OCT image in Figure 1 (e) exhibits broken blood vessels in Figure 1 (h). Fortunately, our proposed Heuristic Contextual Guidance (HCG) module (Figure 1 (g)) effectively addresses this problem.

This paper proposes a TransPro framework to address two problems that exist in the OCT to OCTA image translation. The framework incorporates a VPG module and a HCG module into a 3D image translation baseline through a generative-adversarial learning pattern. The VPG module, discussed in Sec. III-C, is a 2D retinal vascular segmentation model that predicts vessel pixels in 2D OCTA projection maps. During training, semantic consistency is constrained between the vascular segmentation predictions of the translated OCTA images and the ground truth images, enabling the model to pay more attention to vessel regions than non-vessel background regions. Consequently, the *aimlessness in the translation process* problem is addressed. The HCG module, discussed in Sec. III-D, leverages a 2D image translation model to generate 2D OCTA projection maps from paired 2D OCT projection maps. The network transport mechanism with convolutional kernels in a convolutional neural network is used to imbue each pixel of the output with more global contextual information, which is useful for image translation. Thus, the translated 2D OCTA projection maps from the HCG module can provide global contexts for the 3D baseline, guiding the model to handle the *incompleteness of the translated object* problem. The proposed TransPro is evaluated on two subsets of the OCTA-500 public dataset [20], and image quality assessment metrics and two

vessel quality evaluation metrics on the projection map images demonstrate the superiority of the proposed approach over state-of-the-art methods.

The main contributions of this paper are summed up as follows: 1) We propose a new 3D OCT to OCTA image translation framework – TransPro – it can address two potential problems in the existing 3D OCT to OCTA image translation models. 2) TransPro does not require any additional computational overheads during testing. 3) Extensive experimental results validate that TransPro achieves the state-of-the-art accuracy on OCTA-3M and OCTA-6M datasets

## II. RELATED WORK

### A. OCT and OCTA Image Analysis

OCT and OCTA are widely used imaging modalities for diagnosing various retina diseases [1], [4]. OCT enables non-invasive real-time imaging of the three-dimensional cross-sectional structure of the retina, but it does not provide sufficient information for detecting choroidal neovascularization or recognizing the morphological characteristics of microvasculature, which are important for diagnosing retinal diseases [2]. As a complementary modality to OCT, OCTA was introduced to visualize the retinal blood vessels [21], [22]. OCTA images can be generated by detecting temporal signal changes caused by moving red blood cells in multiple OCT images obtained from the same location [7], [23]. However, OCTA devices are expensive and have exclusive sensors, limiting their wider usage. To address this issue, we propose a generative-adversarial learning approach for translating OCT images to OCTA images, which includes a VPG module to enhance the quality of vessel regions and a HCG module to introduce beneficial contextual information.

## B. Modality Translation in Medical Images

In clinical diagnosis, multi-modality images can offer comprehensive and complementary information that can be beneficial for treatment [11], [12]. However, acquiring multi-modality images is challenging due to factors such as cost, time, and potential harm to the body [24]. To overcome this issue, modality translation from an easily obtainable source image modality to a more challenging target image modality is a promising solution. Several generative adversarial network-based methods, such as pix2pix [14] and Cycle GAN [15], have been proposed for modality translation. Among them, OCT to OCTA image translation has been an active research area in recent years, with several methods proposed to address the problem of ambiguity in fine vascular areas of the translated OCTA images [10]–[12]. However, existing methods suffer from aimlessness in the translation process and incompleteness of the translated object. In this paper, we propose a novel approach to tackle these issues by incorporating a vessel promoted guidance module and a heuristic contextual guidance module into the baseline OCT to OCTA image translation model. In this paper, to address these two potential problems, we propose to use a vessel promoted guidance module and a heuristic contextual guidance module on the baseline OCT to OCTA image translation model.

## C. Retinal Vascular Segmentation

Retinal vascular segmentation of OCTA images is a crucial and fundamental task in the diagnosis of retinal diseases. The segmentation provides information on the density and morphological structures of retinal capillary networks, which can be utilized for disease diagnosis or robotic surgery [13]. Various methods have been proposed for retinal vascular segmentation based on the classical UNet framework in recent years [20], [25], [26]. For instance, CSNet adds self-attention blocks to the encoder and decoder network to emphasize curvilinear vessel structures [26]. Besides, DCSSNet is designed as a semi-supervised segmentation model that uses both labeled and unlabeled images to mitigate the high cost of pixel-level annotations [27]. Existing methods consider retinal vascular segmentation as an independent medical image analysis task and treat model design and downstream tasks separately. In contrast, our work treats OCTA vascular segmentation as an auxiliary task to enhance the quality of vascular regions in the translated OCTA images, rather than solely solving the vascular segmentation problem. This approach provides a novel perspective and demonstrates the potential of OCTA vascular segmentation as an auxiliary task.

## D. Multi-Task Learning

Multi-task learning is a widely-used approach that aims to optimize a machine learning model for multiple tasks in a unified framework [28]. It employs shared feature representations to achieve balanced optimization for all the tasks [29]. Despite differences in the requirements for image features, combining adjacent tasks such as object detection and instance segmentation has shown remarkable empirical results [17],

[18]. In cases where tasks have unequal importance, auxiliary learning, where auxiliary tasks are used to assist the main tasks in achieving better predictions, can be employed [30], [31]. Auxiliary tasks are frequently used in generative adversarial networks, such as classification and jigsaw solving [32], [33]. In our method, we use two auxiliary tasks, vascular segmentation and 2D OCTA projection map translation, to help the main task, OCT to OCTA image translation, learn rich feature representations. We integrate all tasks into the same framework and train them in an end-to-end fashion. Our contribution is using two auxiliary tasks to improve the performance of the main task. The coherence between the auxiliary tasks and the main task in terms of features enhances the performance of OCT to OCTA image translation.

## III. METHODOLOGY

As illustrated in Figure 2 (b), the proposed TransPro mainly contains the following three components: 1) a 3D conditional generative adversarial network in Sec. III-A, which is the main body of our method, 2) a Vessel Promoted Guidance (VPG) module in Sec. III-C to solve the *aimlessness in translation process* problem, and 3) a Heuristic Contextual Guidance (HCG) module in Sec. III-D to handle the *incompleteness of translation object* problem.

### A. Preliminaries

OCT to OCTA image translation task aims to translate an OCT volume  $\mathbf{X} \in \mathbb{R}^{D \times H \times W}$  to its paired OCTA volume  $\hat{\mathbf{Y}} \in \mathbb{R}^{D \times H \times W}$ , where the translated OCTA volume  $\hat{\mathbf{Y}}$  needs to be as close as possible to the ground-truth OCTA volume  $\mathbf{Y} \in \mathbb{R}^{D \times H \times W}$  [3]. In particular, each volume data is composed of a set of 2D slices with the size of  $H \times W$  (i.e., B-scan images) and the number of slices for each volume is  $D$ .

Our proposed framework builds upon the classical image-to-image translation model, pix2pix [14]. Unlike existing methods that only consider the OCT B-scan image as input to the generator to produce the corresponding OCTA B-scan image [21], [22], we extend the network to three-dimensional convolutional neural networks to handle 3D volumes and enhance the global contextual learning across slices. Specifically, the input to the 3D generator is a 3D OCT volume and the output is a translated OCTA volume. Additionally, a 3D discriminator is used to differentiate between ground-truth and translated OCTA volumes. The 3D generator and discriminator are denoted as  $G_{3d}$  and  $D_{3d}$ , respectively, and the adversarial loss is formulated accordingly:

$$\mathcal{L}_{Adv3d} = \mathbb{E}_{\mathbf{Y} \sim p(OCTA)} [\log(D_{3d}(\mathbf{Y}))] + \mathbb{E}_{\mathbf{X} \sim p(OCT)} [\log(1 - (D_{3d}(G_{3d}(\mathbf{X})))], \quad (1)$$

where  $\mathbf{Y}$  denotes the ground-truth OCTA volume sampled from distribution  $p(OCTA)$  and  $\mathbf{X}$  denotes the input OCT volume sampled from distribution  $p(OCT)$ .  $G_{3d}(\mathbf{X})$  which is equal to  $\hat{\mathbf{Y}}$ , denotes the output OCTA volume translated by  $G_{3d}$  network. In addition, there is a constraint on each voxel between the translated volume  $G_{3d}(\mathbf{X})$  and the ground-truth



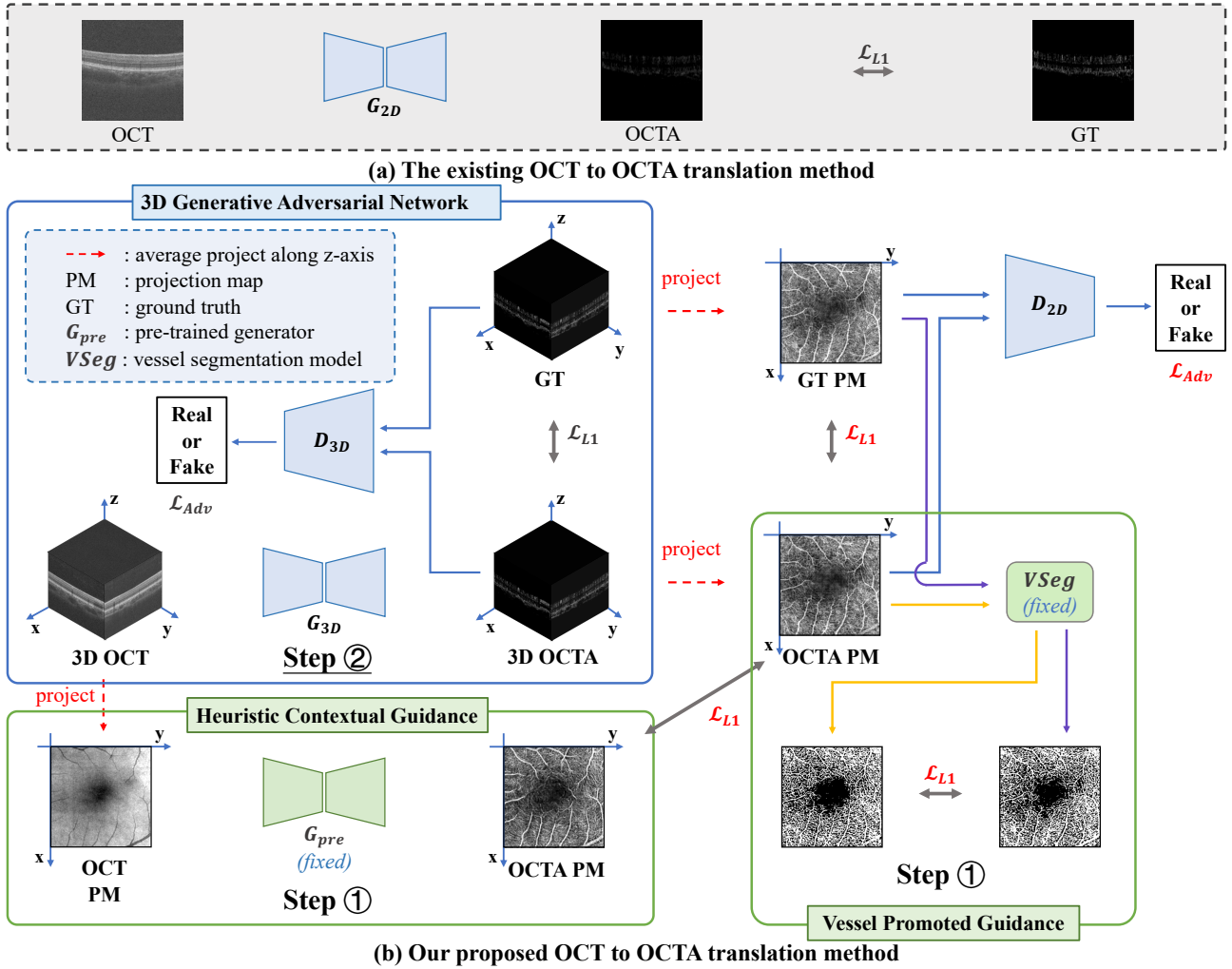


Fig. 2: The main ideas and contributions of this work. (a) illustrates the overall framework of the existing OCT to OCTA translation methods. (b) illustrates our proposed TransPro. Compared to existing methods, TransPro not only takes into considerations of critical vessel information via the Vessel-Promoted Guidance model but also introduces beneficial heuristic contexts via the Heuristic Contextual Guidance model. Therefore, problems of the *aimlessness in the translation process* and the *incompleteness of the translated object* can be addressed.

volume  $\mathbf{Y}$ . To ensure less blurring, we follow [14] and apply  $L1$  distance instead of  $L2$ , which is formulated as:

$$\mathcal{L}_{L13d} = \|\mathbf{Y} - G_{3d}(\mathbf{X})\|_1. \quad (2)$$

The overall loss function for the 3D generative adversarial network is expressed as:

$$\mathcal{L}_{3DGAN} = \mathcal{L}_{Adv3d} + \lambda \mathcal{L}_{L13d}, \quad (3)$$

where  $\lambda$  is a loss-balance hyperparameter which is set to 10 in our experiments.

### B. Overview

The overall framework of our proposed TransPro method is shown in Figure 2 (b), which consists of three parts. The main body is a 3D generative adversarial network with 3D OCT volume  $\mathbf{X}$  as input and 3D OCTA volume  $\hat{\mathbf{Y}}$  as output. To further enhance the quality of translated OCTA volume in the projection view, we design two modules, *i.e.*, VPG and HCG, to handle two problems, respectively. For VPG module

(*Ref III-C*), we have a vascular segmentation model with 2D OCTA projection map as input. For HCG module (*Ref III-D*), we have a 2D OCTA projection map generator with 2D OCT projection map as input. We pre-train the models for VPG and HCG modules and fix their parameters when training the 3D generative adversarial network.

During training, we jointly train the generator  $G_{3d}$  and two discriminators  $D_{3d}$  and  $D_{2d}$  following the generative-adversarial learning pattern [14], [15]. Our total loss function can be formulated as:

$$\mathcal{L}_{TransPro} = \mathcal{L}_{3DGAN} + \mathcal{L}_{VPG} + \mathcal{L}_{HCG}. \quad (4)$$

The final objective function is expressed as:

$$G_{3d}^* = \arg \min_{G_{3d}} \max_{D_{3d}, D_{2d}} \mathcal{L}_{TransPro}(G_{3d}, D_{3d}, D_{2d}). \quad (5)$$

In inference, only the 3D generator  $G_{3d}$  is used. Therefore, TransPro does not require any additional computational overheads in this process. The implementation details of VPG and HCG modules are introduced in following two sections.

### C. Vessel Promoted Guidance (VPG)

Given that OCTA images are primarily used to reflect vessel signals, the similarity of blood vessels between synthesized and ground truth data is more crucial than the similarity of background tissues. However, it is challenging for the network to focus on vessel pixels in the absence of specific flow information [7], [23]. Thus, we introduce a vessel segmentation model with fixed parameters to guide the generation accuracy of vessel regions. In addition to the 3D view ( $D \times H \times W$ ), there is another 2D projection view ( $D \times W$ ) of OCTA volumetric data that is capable of visualizing vascular structures. We obtain the 2D OCTA projection maps by averaging the values of pixels along the  $H$  dimension. The projection process is represented as  $Proj(\cdot)$ , and the obtained OCTA projection map is denoted as  $\hat{\mathbf{y}} \in \mathbb{R}^{D \times W}$ , then we have:

$$\hat{\mathbf{y}} = Proj(\hat{\mathbf{Y}}). \quad (6)$$

Based on experimental observations, it has been noted that the constraints in Eq. 3 may not be sufficient to ensure high quality in the translated OCTA projection maps. The reason behind this is the accumulation of errors during the computation of projection maps of the translated OCTA volumes with Eq. 6. Therefore, to enhance the similarity between the ground-truth and translated OCTA projection maps, we propose the use of a 2D adversarial loss (referred to as  $\mathcal{L}_{Adv2d}$ ) and L1 loss (referred to as  $\mathcal{L}_{proj}$ ). To achieve this, we apply the projection function  $Proj(\cdot)$  on the ground-truth OCTA volume  $\mathbf{Y}$  and the translated OCTA volume  $\hat{\mathbf{Y}}$  to obtain the corresponding ground-truth and translated projection maps, denoted as  $\mathbf{y}$  and  $\hat{\mathbf{y}}$ , respectively. The losses are then computed as follows:

$$\begin{aligned} \mathcal{L}_{Adv2d} = & \mathbb{E}_{\mathbf{Y} \sim p(OCTA)}[\log(D_{2d}(\mathbf{y}))] \\ & + \mathbb{E}_{\hat{\mathbf{Y}} \sim p(OCT)}[\log(1 - (D_{2d}(\hat{\mathbf{y}})))] \end{aligned} \quad (7)$$

$$\mathcal{L}_{proj}(G_{3d}) = \|\mathbf{y} - \hat{\mathbf{y}}\|_1, \quad (8)$$

where

$$\begin{aligned} \mathbf{y} &= Proj(\mathbf{Y}), \\ \hat{\mathbf{y}} &= Proj(\hat{\mathbf{Y}}) = Proj(G_{3d}(\mathbf{X})). \end{aligned} \quad (9)$$

$D_{2d}$  denotes a 2D discriminator which differentiates the ground-truth and translated OCTA projection maps.

Moreover, during the 3D volume translation process, the lack of vessel information leads to aimlessness, resulting in poor quality of vascular regions in translated OCTA projection maps. To this end, we propose a vascular segmentation model to focus more on the vascular regions. Initially, we pre-train a vascular segmentation model  $VSeg(\cdot)$  on OCTA projection maps with annotated vessel labels. Next, we use  $VSeg(\cdot)$  to extract semantic vascular segmentation logits on both ground-truth and translated OCTA projection maps, denoted as  $\mathbf{I}_{seg}$  and  $\hat{\mathbf{I}}_{seg}$ , respectively. Finally, we employ L1 distance to minimize the discrepancy between the two logits:

$$\mathcal{L}_{seg} = \alpha \left\| \hat{\mathbf{I}}_{seg} - \mathbf{I}_{seg} \right\|_1, \quad (10)$$

where

$$\begin{aligned} \hat{\mathbf{I}}_{seg} &= VSeg(Proj(G_{3d}(\mathbf{X}))), \\ \mathbf{I}_{seg} &= VSeg(Proj(\mathbf{Y})), \end{aligned} \quad (11)$$

and  $\alpha$  is the weight of  $\mathcal{L}_{seg}$  which is set to 5.

The  $\mathcal{L}_{seg}$  loss aims to match the vascular structures in the ground-truth and translated OCTA projection maps, addressing the problem of aimlessness in the translation process. To this end, we combine the losses in Eq. 7, Eq. 8, and Eq. 10 into a single loss function  $\mathcal{L}_{VPG}$  for the VPG module:

$$\mathcal{L}_{VPG}(G_{3d}, D_{2d}) = \mathcal{L}_{Adv2d} + \lambda \mathcal{L}_{proj} + \mathcal{L}_{seg} \quad (12)$$

### D. Heuristic Contextual Guidance (HCG)

The constraint in Eq. 8 restricts the ground-truth 2D OCTA projection map, leading to incomplete vessels in the translated results. Since ground-truth images only provide hard labels for each pixel, they do not consider neighboring contextual information which is essential for translating unbroken vessels [18], [26]. To address this problem, we propose generating a sub-optimal (*i.e.*, the heuristic) 2D OCTA projection map that can provide heuristic contextual information. Furthermore, we utilize the properties of convolutional kernels in the convolutional neural network. Each output value considers the surrounding pixels, resulting in outputs that contain more contextual information. This information can guide the translation of long vascular structures across multiple slices. Consequently, we design a 2D generation model to generate OCTA projection maps from their paired OCT projection maps.

Specifically, the pre-trained model's generator ( $G_{pre}$ ) is utilized and its parameters are fixed during training. The projection map of the input OCT volume is then subjected to  $G_{pre}$ , resulting in an OCTA projection map that contains contextual information. The output of the 2D translation model,  $G_{pre}$ , is denoted as  $\mathbf{y}'$ . The L1 distance is utilized to determine the dissimilarity between  $\mathbf{y}'$  and the projection map of translated OCTA,  $G_{3d}(\mathbf{X})$ , which is produced by  $G_{3d}$ , which can be formulated as:

$$\mathcal{L}_{HCG}(G_{3d}) = \beta \|\mathbf{y}' - Proj(G_{3d}(\mathbf{X}))\|_1, \quad (13)$$

where

$$\mathbf{y}' = G_{pre}(Proj(\mathbf{X})), \quad (14)$$

and  $\beta$  is the weight of  $\mathcal{L}_{HCG}$  which is set to 5.

## IV. EXPERIMENTS

### A. Datasets

**OCTA-500 dataset.** OCTA-500 [20] is a publicly accessible dataset with 500 pairs of 3D OCT and OCTA volumes. This dataset is divided into two subsets according to the field of view types, which are OCTA-3M and OCTA-6M, respectively. We implement our model on these two subsets.

- **OCTA-3M** contains 200 pairs of OCT and OCTA volumes with  $3\text{mm} \times 2\text{mm} \times 3\text{mm}$  field of view. Each volume is with the size of  $304\text{px} \times 640\text{px} \times 304\text{px}$ , and the size of the projection map is  $304\text{px} \times 304\text{px}$ . Following [20], we divide the size of the training set, validation set, and test set as 140 volumes, 10 volumes, and 50 volumes, respectively.
- **OCTA-6M** contains 300 pairs of OCT and OCTA volumes with  $6\text{mm} \times 2\text{mm} \times 6\text{mm}$  field of view. The

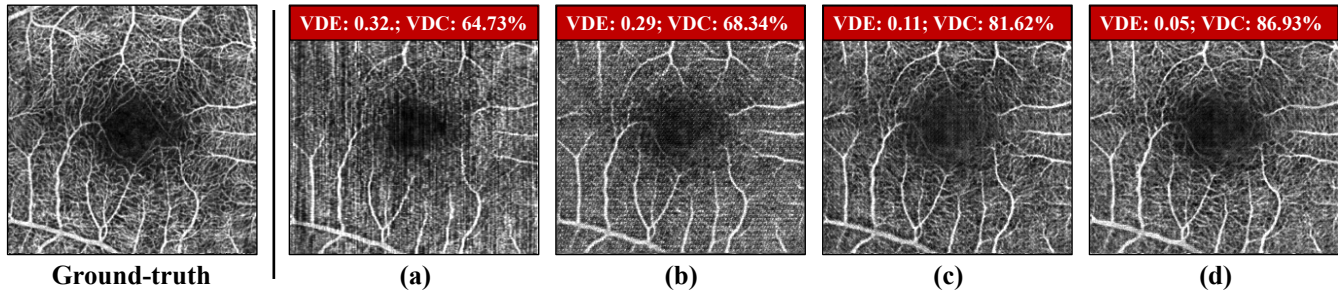


Fig. 3: The OCTA projection maps with different vessel density error (VDE) and vessel density correlation (VDC) results. The leftmost side is the ground-truth and (a)-(d) are the four translated OCTA projection maps with different qualities from low to high. The results of VDE and VDC metrics are matched with the visualized quality.

volume is with the size of  $400\text{px} \times 640\text{px} \times 400\text{px}$ , and the size of its projection map is  $400\text{px} \times 400\text{px}$ . The size of the training set, validation set, and test set for the OCTA-6M dataset is 180 volumes, 20 volumes, and 100 volumes, respectively.

### B. Evaluation Metrics

We evaluate the translated OCTA images from the following two aspects: OCTA volume and OCTA projection map. To evaluate the quality of OCTA volume, we use standard image quality assessment metrics, *i.e.*, Mean Absolute Error (MAE), Peak Signal-to-Noise Ratio (PSNR) [34], and Structural Similarity (SSIM) [35] and average the results over each slide of the whole volume (B-scan image).

In addition to the standard evaluation metrics used to assess the quality of OCTA volume, we have implemented five supplementary evaluation metrics on the OCTA projection map to measure the similarity of vessels that may not be directly visible in the OCTA volumes. These metrics have been modified from the Mean Absolute Error (MAE), Peak Signal-to-Noise Ratio (PSNR), and Structural Similarity (SSIM) metrics and are now referred to as vessel-weighted metrics. We denote these metrics as MAE-V, PSNR-V, and SSIM-V. To calculate the vessel-weighted metrics between the translated and ground-truth OCTA projection maps, we multiply the value of non-vessel pixels by a ratio  $\gamma \in (0, 1.0]$ , while the vessel pixels remain unchanged. We have set the value of  $\gamma$  to 0.1 for the results presented in Table II. Additionally, we have provided results for the MAE-V, PSNR-V, and SSIM-V metrics for other values of  $\gamma$  in Section IV-E2.

Another significant factor for evaluating OCTA projection maps is vessel density [36], which is a vital parameter in detecting vessel abnormalities in various retinal diseases, particularly in their early phases [37]–[39]. The calculation of vessel density is based on the proportion of the vessel area over the total area, which can be expressed as the percentage of vessel pixels over the total pixels within a given region [40]. In this study, we propose two metrics that utilize vessel density to quantify the similarity between the translated and ground-truth OCTA projection maps. The design of these metrics aims to further enhance the assessment of the quality of vascular regions in the OCTA images.

- **Vessel Density Error (VDE).** The VDE metric is utilized to assess the absolute discrepancies of vessel densities between translated and ground-truth OCTA projection maps. As shown in Figure 3, lower VDE values indicate better quality of the translation outcomes.
- **Vessel Density Correlation (VDC).** VDC is employed to assess the similarity of vessel density in a local-wise manner. Specifically, we partition each OCTA projection map into small patches of size  $16\text{px} \times 16\text{px}$ , compute the vessel density for each patch, and derive a vector of regional vessel densities. We then calculate the Pearson correlation coefficient of the two vectors as VDC between the translated and ground-truth OCTA projection maps. Experimental results in Figure 3 validate that a higher VDC corresponds to a better translation quality.

### C. Implementation Details

**Settings.** We first train two models for VPG and HCG and freeze their parameters to train our proposed TransPro model. The backbones and the detailed training settings for each component are introduced below.

- **VPG.** We utilize the UNet [13] as the underlying model for the vascular segmentation module in the VPG framework. This module aims to generate predictions of vascular segmentation in OCTA projection maps, using vessel pixel annotations as the ground-truth labels. We adopt five-fold cross-validation. For data augmentation, we divide each projection map into 16 patches and resize them to  $256\text{px} \times 256\text{px}$  before training. Consequently, the size of the training set is increased to 128. During the training process, we apply common data augmentation methods such as random cropping and flipping. The model is trained with cross-entropy loss using RMSprop optimizer with a learning rate of  $10^{-5}$  for 100 epochs.
- **HCG.** We apply the pix2pix [14] as the backbone of the OCT to OCTA projection map translation model for HCG module. The projection maps of OCT and OCTA volumes are computed by the projection function  $Proj(\cdot)$  in Equation 6. The splitting of training, validation, and test sets is consistent with original 3D datasets. We follow the settings in [14] and train the model over 200 epochs. After training, we select the model with the best result on the validation set.



TABLE I: Result comparisons with the state-of-the-arts on OCTA volumes of OCTA-3M and OCTA-6M [20]. Results of other methods are produced by our re-implementation. “↓” refers to the lower the better and “↑” refers to the higher the better.

Method	OCTA-3M Dataset			OCTA-6M Dataset		
	MAE ↓	PSNR(dB) ↑	SSIM(%) ↑	MAE ↓	PSNR(dB) ↑	SSIM(%) ↑
Pix2pix 2D [14]	0.0968	29.59	84.59	0.0995	27.65	87.15
Pix2pix 3D [14]	0.0883	31.58	86.24	0.0900	<b>30.66</b>	87.16
9B18CN UNet [10]	0.0918	29.34	86.04	0.1135	27.91	83.69
Adjacent GAN [12]	0.0906	30.89	87.14	0.1021	28.05	85.03
<b>TransPro (ours)</b>	<b>0.0782</b>	<b>32.56</b>	<b>88.22</b>	<b>0.0854</b>	30.53	<b>88.35</b>

TABLE II: Result comparisons with the state-of-the-arts on OCTA projections of OCTA-3M and OCTA-6M [20]. Results of other methods are produced by our re-implementation. “↓” refers to the lower the better and “↑” refers to the higher the better.

Method	OCTA-3M Dataset					OCTA-6M Dataset				
	MAE-V ↓	PSNR-V(dB) ↑	SSIM-V(%) ↑	VDE ↓	VDC(%) ↑	MAE-V ↓	PSNR-V(dB) ↑	SSIM-V(%) ↑	VDE ↓	VDC(%) ↑
Pix2pix 2D [14]	0.0823	17.92	85.26	0.2996	61.78	0.0845	16.72	85.47	0.3276	63.72
Pix2pix 3D [14]	0.0753	20.36	89.14	0.1836	63.20	0.0923	17.04	84.51	0.3400	69.48
9B18CN UNet [10]	0.0839	17.12	85.03	0.3188	59.92	0.0895	16.89	84.07	0.3112	62.81
Adjacent GAN [12]	0.0833	17.56	85.88	0.3026	62.34	0.0879	17.19	84.44	0.3204	65.79
<b>TransPro (ours)</b>	<b>0.0658</b>	<b>20.42</b>	<b>91.79</b>	<b>0.0668</b>	<b>81.94</b>	<b>0.0733</b>	<b>17.20</b>	<b>90.23</b>	<b>0.0776</b>	<b>80.43</b>

- **TransPro.** Upon completion of training the VPG and HCG modules, we proceed with training the TransPro model. The 3D pix2pix model, a modified version of the model proposed in [14], is used as the backbone of TransPro. In this setup, the 3D generator  $G_{3d}$  and two discriminators  $D_{3d}$  and  $D_{2d}$  are jointly trained following the adversarial-learning manner. We use Adam optimizer and set the initial learning rate to 0.0002. The model is trained with a batch size of 1 for 200 epochs. To prevent overfitting, we evaluate the validation set using mean absolute error and select the best model with the minimum error value.

#### D. Comparisons with the State-of-the-art Methods

We re-implemented several state-of-the-art methods for OCT to OCTA image translation. The results of the comparisons of our proposed TransPro and other methods on three datasets are summarized in Table I and II. Table I shows the experimental results of MAE, PSNR, and SSIM on OCTA B-scan images, and Table II displays the experimental results of vessel density error (VDE) and vessel density correlation (VDC) on OCTA projection maps.

1) *OCTA-3M*: We compare our TransPro with two baseline methods and two methods proposed for OCT to OCTA image translation. The two baseline methods, *i.e.*, pix2pix 2D and pix2pix 3D are implemented follow the network architectures in [14]. The inputs and outputs of pix2pix 2D method are the paired OCT and OCTA B-scan images while they are the paired OCT and OCTA volumes for pix2pix 3D method. Besides, Adjacent GAN [12] utilizes three adjacent B-scan images during training, while pix2pix 2D [14] and 9B18CN UNet [10] use the single B-scan image for training. Among the four compared methods, pix2pix 3D [14] is trained on 3D volumes while the other three methods are trained on 2D b-scan images. From the results, we find that pix2pix 3D performs better than Adjacent GAN, while Adjacent GAN is better than pix2pix 2D and 9B18CN UNet methods. This

indicates the importance of inter-slice connections which provide more global information than a single B-scan image. In addition to the 3D spatial information, our proposed TransPro method integrates vessel and contextual guidance from VPG and HCG modules. Therefore, TransPro obtains significant improvements in the OCTA-3M dataset compared with other methods in both B-scan images and the projection maps. Especially for VDE and VDC metrics, as shown in Table II, our method enhances over pix2pix 3D model by 0.1168 and 18.74%, respectively.

2) *OCTA-6M*: We conduct the experiments of our proposed TransPro and four other methods on the OCTA-6M dataset. In general, the quality of translated images in the OCTA-6M dataset is lower than the images in the OCTA-3M dataset. This may cause by the lower resolution of images due to the larger field of view in the OCTA-6M dataset. For the results among the four compared methods, the outcomes are consistent with the OCTA-3M dataset, where the performance is positively correlated with the degree of global information utilized by the model. Our proposed TransPro achieves the best performance among all the compared methods except that the PSNR value is slightly lower than the result of the Pix2pix 3D model. The remarkable improvements of VDE and VDC metrics which are applied to OCTA projection maps show the effectiveness of our method in enhancing the quality of vascular structures.

3) *Visualization quality*: To evaluate the results qualitatively, we provide some visualization examples of OCTA projection maps translated by different methods. As shown in Figure 4, we choose two images from OCTA-3M and OCTA-6M datasets respectively, and compare the results of our proposed TransPro with Pix2pix 3D and Adjacent GAN methods. From the enlarged figures, we find that the Pix2pix 3D model generates some artifacts to mimic the texture of vessels while the outputs of the Adjacent GAN model suffer from white stripes due to the limited intra-slice information of the 2D model. Compared to the ambiguous images translated from other methods, our method produces high-quality OCTA projection images with vivid vessels and background tissues.

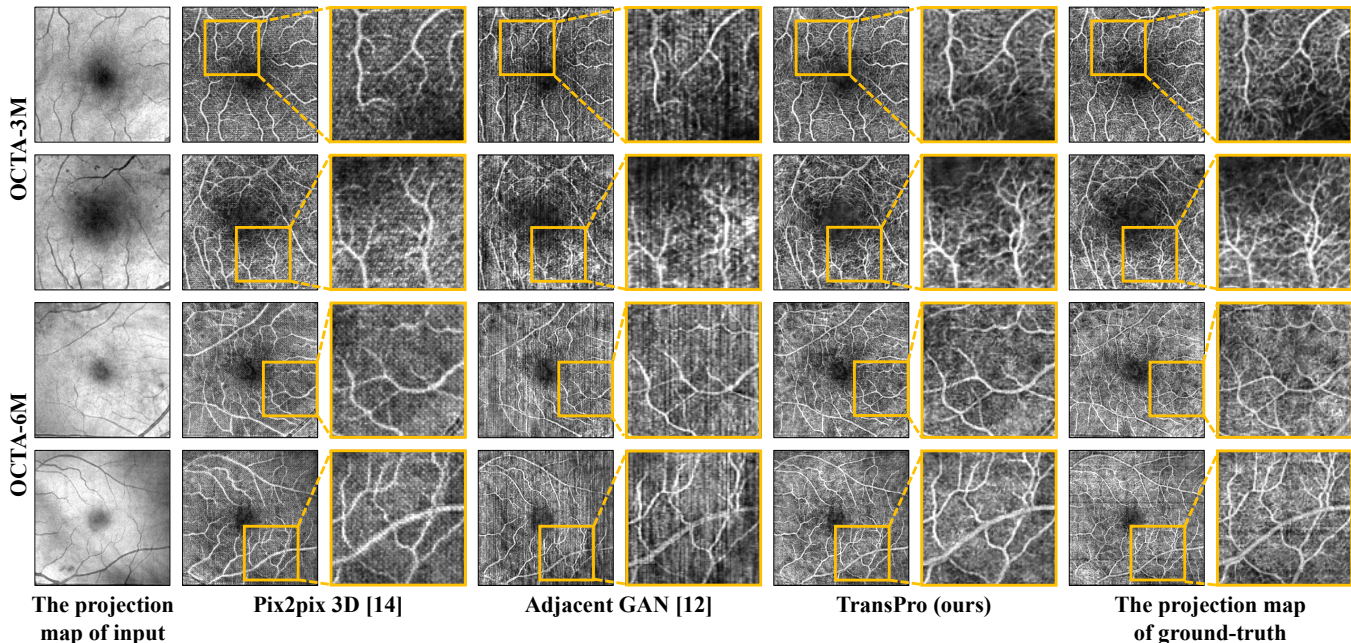


Fig. 4: Visualization result comparisons of translated OCTA projection maps in OCTA-3M dataset and OCTA-6M [20]. Two examples are selected from each dataset correspondingly. We can observe that our approach can achieve better predictions.

TABLE III: Ablation studies on the effectiveness of VPG and HCG modules on OCTA-3M and OCTA-6M [20]. The MAE, PSNR (dB) and SSIM (%) are computed on OCTA volumes, while the VDE and VDC (%) are computed on OCTA projection maps. “↓” refers to the lower the better and “↑” refers to the higher the better.

3D GAN	VPG	HCG	MAE ↓	PSNR(dB) ↑	SSIM(%) ↑	VDE ↓	VDC(%) ↑
OCTA-3M Dataset							
✓			0.0883	31.5824	86.24	0.1836	63.20
✓	✓		0.0807	32.4794	87.43	0.2039	70.68
✓		✓	0.0797	31.9813	87.78	0.1808	68.10
✓	✓	✓	<b>0.0782</b>	<b>32.5587</b>	<b>88.22</b>	<b>0.0668</b>	<b>81.94</b>
OCTA-6M Dataset							
✓			0.0900	<b>30.6621</b>	87.16	0.3400	69.48
✓	✓		0.0879	30.1424	88.15	0.3067	70.87
✓		✓	0.0860	29.8427	88.24	0.2672	70.02
✓	✓	✓	<b>0.0854</b>	30.5264	<b>88.35</b>	<b>0.0776</b>	<b>80.43</b>

E. Ablation Study

1) *Effectiveness of VPG and HCG modules:* To validate the respective effectiveness of VPG and HCG components, we conduct additional experiments by separately adding these two modules to the 3D GAN baseline model. Table III displays the results on OCTA-3M and OCTA-6M datasets. In general, we can find that VPG and HCG modules bring improvement to the quality of B-scan images as the metrics of MAE, PSNR and SSIM evaluating OCTA B-scan images become better after adding corresponding components. For the quality of projection maps of translated OCTA images, the vessel density error (VDE) and vessel density correlation (VDC) metrics indicate the effectiveness of VPG and HCG modules on vascular areas. In particular, VPG module shows more improvement on VDC metric because it provides the semantic vascular segmentation map which increases the similarity of overall vascular structures. HCG module pays more attention to the guidance of pixel-wise contextual information, hence it gains a significant drop on VDE metric, especially for

the OCTA-6M dataset. Moreover, when the VPG and HCG modules are applied simultaneously on the baseline model, *i.e.*, our proposed TransPro framework, the performance obtains prominent gains compared to the results with either VPG or HCG module. Therefore, we conclude that VPG and HCG modules offer their own effectiveness on the OCT to OCTA image translation task and their effects are additive when the two modules are active in TransPro method.

2) *Evaluation of translated vascular quality:* To evaluate the quality of translated vessels in OCTA projection maps, we further calculate vessel-weighted MAE, PSNR, and SSIM metrics by adjusting the ratio of pixel weights between vessel pixels and non-vessel pixels according to the vessel segmentation mask. We summarize the results in line charts for different ratios in OCTA-3M and OCTA-6M datasets, as shown in Fig 5 and 6, respectively. Specifically, we first obtain the pixel-wise vascular labels of OCTA projection maps in the test set which are annotated by ophthalmologists. Then, for the non-vessel pixels in the segmentation mask, we multiply the



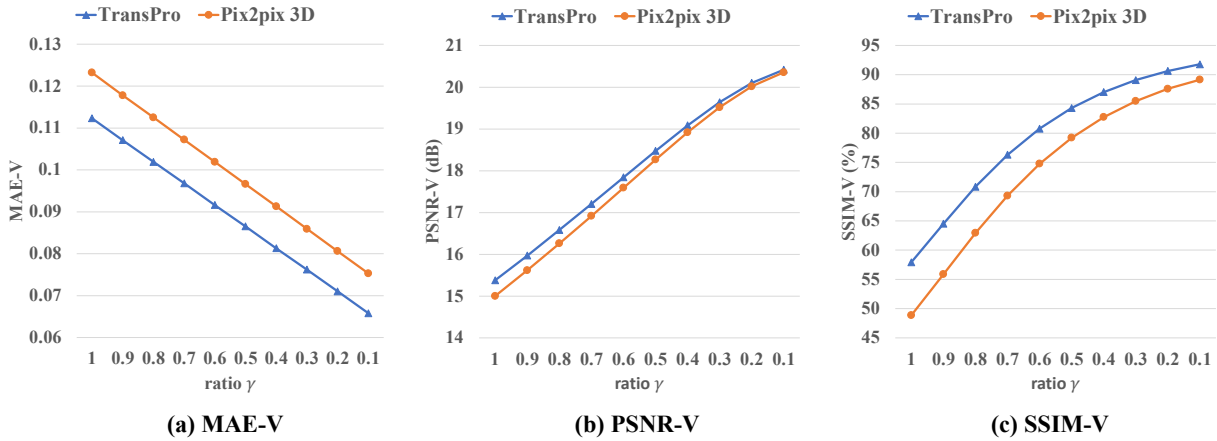


Fig. 5: Evaluation of translated vascular quality on OCTA projection in OCTA-3M [20]. The non-vascular pixels are multiplied by a ratio  $\gamma$  from 1.0 to 0.1. The three evaluation metrics, *i.e.*, (a) MAE-V, (b) PSNR-V and (c) SSIM-V, are computed on processed OCTA projection maps. The x-axis refers to the coefficient multiplied to non-vascular pixels, and the y-axis refers to the results of corresponding metrics.

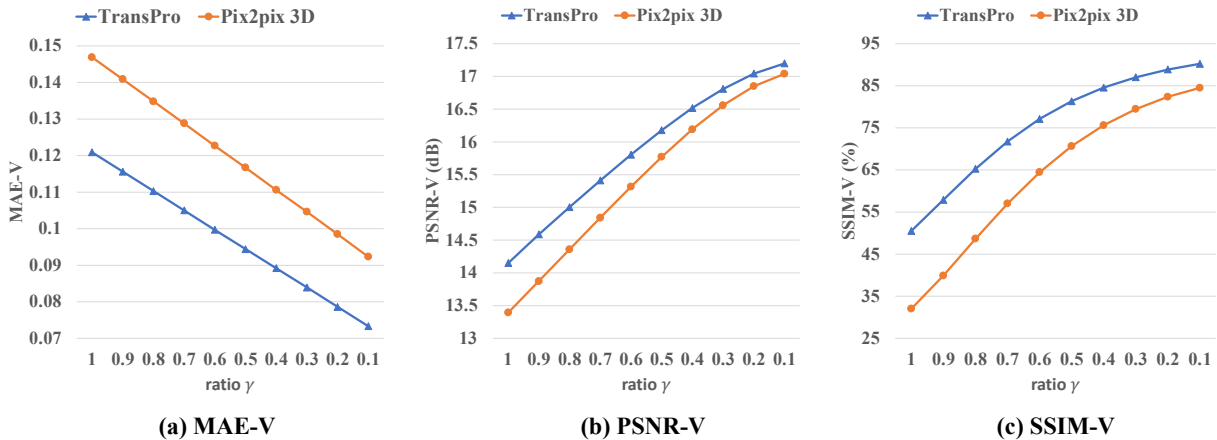


Fig. 6: Evaluation of translated vascular quality on OCTA projection in OCTA-6M [20]. The non-vascular pixels are multiplied by a ratio  $\gamma$  from 1.0 to 0.1. The three evaluation metrics, *i.e.*, (a) MAE-V, (b) PSNR-V and (c) SSIM-V, are computed on processed OCTA projection maps. The x-axis refers to the coefficient multiplied to non-vascular pixels, and the y-axis refers to the results of corresponding metrics.

OCTA projection maps by a ratio  $\gamma \in \{1.0, 0.9, \dots, 0.1\}$  to gradually decrease the weights of non-vessel pixels from 1.0 to 0.1. The weights of vessel pixels remain at 1.0. We apply the weights adjusting for all translated OCTA projection maps and the ground-truth images and compute MAE-V, PSNR-V, and SSIM-V metrics between two sets of projection maps. In consequence, as the weights of vascular pixels increase, MAE-V drops linearly and the metric of PSNR-V and SSIM-V gradually improve for both OCTA-3M and OCTA-6M datasets. In particular, the PSNR-V and SSIM-V results of TransPro method can achieve over 20 dB and 90% for the OCTA-3M dataset and over 17 dB and 90% for the OCTA-6M dataset, respectively, when the weights of non-vessel pixels reduce to 0.1. In addition, by comparing our method to Pix2pix 3D method on both two datasets, the results indicate that our method can achieve higher quality in both non-vessel regions (when the ratio is high) and vessel regions (when the ratio is low) than pix2pix 3D model.

## V. CONCLUSION

In this paper, a novel framework to 3D OCT to OCTA image translation, termed TransPro, is proposed. TransPro leverages a generative-adversarial learning approach to address two potential issues that may arise in the translation process: aimlessness and incompleteness of the translated object. To address these problems, two corresponding modules, namely VPG and HCG, are introduced. The former provides semantic vascular information to encourage the model to pay more attention to vascular regions, while the latter addresses the incompleteness of volumetric data among slices by incorporating contextual information. Experimental results on public datasets demonstrate that TransPro achieves outstanding performance. TransPro is a versatile 3D image generation model that can be applied to a wide range of computer vision tasks, such as data augmentation, semantic segmentation, and domain adaptation. Future work will explore the use of TransPro in additional image generation applications.

## REFERENCES

- [1] D. Huang, E. A. Swanson, C. P. Lin, J. S. Schuman, W. G. Stinson, W. Chang, M. R. Hee, T. Flotte, K. Gregory, C. A. Puliafito, and J. G. Fujimoto, "Optical coherence tomography," *Science*, vol. 254, no. 5035, pp. 1178–1181, 1991.
- [2] R. F. Spaide, J. G. Fujimoto, N. K. Waheed, S. R. Sadda, and G. Staurengi, "Optical coherence tomography angiography," *Progress in Retinal and Eye Research*, vol. 64, pp. 1–55, 2018.
- [3] D. Yang, A. R. Ran, T. X. Nguyen, T. P. Lin, H. Chen, T. Y. Lai, C. C. Tham, and C. Y. Cheung, "Deep learning in optical coherence tomography angiography: Current progress, challenges, and future directions," *Diagnostics*, vol. 13, no. 2, p. 326, 2023.
- [4] J. Fujimoto and E. Swanson, "The development, commercialization, and impact of optical coherence tomography," *Investigative Ophthalmology & Visual Science*, vol. 57, no. 9, pp. OCT1–OCT13, 2016.
- [5] X. Li, H. Chen, X. Qi, Q. Dou, C.-W. Fu, and P.-A. Heng, "H-denseunet: hybrid densely connected unet for liver and tumor segmentation from ct volumes," *IEEE Transactions on Medical Imaging*, vol. 37, no. 12, pp. 2663–2674, 2018.
- [6] G. Kim, J. Kim, W. J. Choi, C. Kim, and S. Lee, "Integrated deep learning framework for accelerated optical coherence tomography angiography," *Scientific Reports*, vol. 12, no. 1, p. 1289, 2022.
- [7] A. H. Kashani, C.-L. Chen, J. K. Gahm, F. Zheng, G. M. Richter, P. J. Rosenfeld, Y. Shi, and R. K. Wang, "Optical coherence tomography angiography: a comprehensive review of current methods and clinical applications," *Progress in Retinal and Eye Research*, vol. 60, pp. 66–100, 2017.
- [8] L. Lin, Z. Wang, J. Wu, Y. Huang, J. Lyu, P. Cheng, J. Wu, and X. Tang, "Bsda-net: A boundary shape and distance aware joint learning framework for segmenting and classifying octa images," in *International Conference on Medical Image Computing and Computer-Assisted Intervention (MICCAI)*, 2021.
- [9] P. Anvari, M. Ashrafkhorasani, A. Habibi, and K. G. Falavarjani, "Artifacts in optical coherence tomography angiography," *Journal of Ophthalmic & Vision Research*, vol. 16, no. 2, p. 271, 2021.
- [10] C. S. Lee, A. J. Tyring, Y. Wu, S. Xiao, A. S. Rokem, N. P. DeRuyter, Q. Zhang, A. Tufail, R. K. Wang, and A. Y. Lee, "Generating retinal flow maps from structural optical coherence tomography with artificial intelligence," *Scientific Reports*, vol. 9, no. 1, pp. 1–11, 2019.
- [11] Z. Zhang, Z. Ji, Q. Chen, S. Yuan, and W. Fan, "Texture-guided u-net for oct-to-octa generation," in *Chinese Conference on Pattern Recognition and Computer Vision (PRCV)*, 2021.
- [12] P. L. Li, C. O'Neil, S. Saberi, K. Sinder, K. Wang, B. Tan, Z. Hosseinaee, K. Bizhevat, and V. Lakshminarayanan, "Deep learning algorithm for generating optical coherence tomography angiography (octa) maps of the retinal vasculature," *Applications of Machine Learning*, vol. 11511, pp. 39–49, 2020.
- [13] O. Ronneberger, P. Fischer, and T. Brox, "U-net: Convolutional networks for biomedical image segmentation," in *International Conference on Medical Image Computing and Computer-Assisted Intervention (MICCAI)*, 2015.
- [14] P. Isola, J. Zhu, T. Zhou, and A. A. Efros, "Image-to-image translation with conditional adversarial networks," in *IEEE/CVF Conference on Computer Vision and Pattern Recognition (CVPR)*, 2017.
- [15] J. Zhu, T. Park, P. Isola, and A. A. Efros, "Unpaired image-to-image translation using cycle-consistent adversarial networks," in *IEEE/CVF International Conference on Computer Vision (ICCV)*, 2017.
- [16] Y. LeCun, Y. Bengio, and G. Hinton, "Deep learning," *Nature*, vol. 521, no. 7553, pp. 436–444, 2015.
- [17] D. Zhang, H. Zhang, J. Tang, M. Wang, X. Hua, and Q. Sun, "Feature pyramid transformer," in *European Conference on Computer Vision (ECCV)*, 2020.
- [18] D. Zhang, H. Zhang, J. Tang, X.-S. Hua, and Q. Sun, "Self-regulation for semantic segmentation," in *IEEE/CVF International Conference on Computer Vision (ICCV)*, 2021.
- [19] C. Saharia, W. Chan, H. Chang, C. Lee, J. Ho, T. Salimans, D. Fleet, and M. Norouzi, "Palette: Image-to-image diffusion models," in *ACM SIGGRAPH*, 2022.
- [20] M. Li, Y. Zhang, Z. Ji, K. Xie, S. Yuan, Q. Liu, and Q. Chen, "Ipn-v2 and octa-500: Methodology and dataset for retinal image segmentation," in *arXiv*, 2020.
- [21] L. Roisman and R. Goldhardt, "Oct angiography: an upcoming non-invasive tool for diagnosis of age-related macular degeneration," *Current Ophthalmology Reports*, vol. 5, no. 2, pp. 136–140, 2017.
- [22] N. Eladawi, M. Elmogy, F. Khalifa, M. Ghazal, N. Ghazi, A. Aboelfetouh, A. Riad, H. Sandhu, S. Schaal, and A. El-Baz, "Early diabetic retinopathy diagnosis based on local retinal blood vessel analysis in optical coherence tomography angiography (octa) images," *Medical Physics*, vol. 45, no. 10, pp. 4582–4599, 2018.
- [23] D. Ferrara, N. K. Waheed, and J. S. Duker, "Investigating the choriocapillaris and choroidal vasculature with new optical coherence tomography technologies," *Retinal and Eye Research*, vol. 52, pp. 130–155, 2016.
- [24] D. Zhang, Y. Lin, H. Chen, Z. Tian, X. Yang, J. Tang, and K. T. Cheng, "Deep learning for medical image segmentation: tricks, challenges and future directions," *arXiv*, 2022.
- [25] Y. Ma, H. Hao, J. Xie, H. Fu, J. Zhang, J. Yang, Z. Wang, J. Liu, Y. Zheng, and Y. Zhao, "Rose: a retinal oct-angiography vessel segmentation dataset and new model," *IEEE Transactions on Medical Imaging*, vol. 40, no. 3, pp. 928–939, 2020.
- [26] L. Mou, Y. Zhao, L. Chen, J. Cheng, Z. Gu, H. Hao, H. Qi, Y. Zheng, A. Frangi, and J. Liu, "Cs-net: channel and spatial attention network for curvilinear structure segmentation," in *International Conference on Medical Image Computing and Computer-Assisted Intervention (MICCAI)*, 2019.
- [27] Z. Chen, Y. Xiong, H. Wei, R. Zhao, X. Duan, and H. Shen, "Dual-consistency semi-supervision combined with self-supervision for vessel segmentation in retinal octa images," *Biomedical Optics Express*, vol. 13, no. 5, pp. 2824–2834, 2022.
- [28] R. Caruana, "Multitask learning," *Machine Learning*, vol. 28, no. 1, pp. 41–75, 1997.
- [29] R. Li, S. Liu, G. Wang, G. Liu, and B. Zeng, "Jigsawgan: Auxiliary learning for solving jigsaw puzzles with generative adversarial networks," *IEEE Transactions on Image Processing*, vol. 31, pp. 513–524, 2021.
- [30] A. Kendall, Y. Gal, and R. Cipolla, "Multi-task learning using uncertainty to weigh losses for scene geometry and semantics," in *IEEE/CVF Conference on Computer Vision and Pattern Recognition (CVPR)*, 2018.
- [31] S. Liu, E. Johns, and A. J. Davison, "End-to-end multi-task learning with attention," in *IEEE/CVF Conference on Computer Vision and Pattern Recognition (CVPR)*, 2019.
- [32] L. Liebel and M. Körner, "Auxiliary tasks in multi-task learning," in *arXiv*, 2018.
- [33] A. Odena, C. Olah, and J. Shlens, "Conditional image synthesis with auxiliary classifier gans," in *International Conference on Machine Learning (ICML)*, 2017.
- [34] E. Oriani, "qpsnr: A quick psnr/ssim analyzer for linux," <http://qpsnr.youlink.org>, accessed: 2022-11-07.
- [35] Z. Wang, A. C. Bovik, H. R. Sheikh, and E. P. Simoncelli, "Image quality assessment: from error visibility to structural similarity," *IEEE Transactions on Image Processing*, vol. 13, no. 4, pp. 600–612, 2004.
- [36] X. Yao, M. N. Alam, D. Le, and D. Toslak, "Quantitative optical coherence tomography angiography: a review," *Experimental Biology and Medicine*, vol. 245, no. 4, pp. 301–312, 2020.
- [37] R. Mastropasqua, L. Toto, A. Mastropasqua, R. Aloia, C. De Nicola, P. A. Mattei, G. Di Marzio, M. Di Nicola, and L. Di Antonio, "Foveal avascular zone area and parafoveal vessel density measurements in different stages of diabetic retinopathy by optical coherence tomography angiography," *International Journal of Ophthalmology*, vol. 10, no. 10, p. 1545, 2017.
- [38] M. Al-Sheikh, N. A. Iafe, N. Phasukkijwatana, S. R. Sadda, and D. Sarraf, "Biomarkers of neovascular activity in age-related macular degeneration using optical coherence tomography angiography," *Retina*, vol. 38, no. 2, pp. 220–230, 2018.
- [39] G. M. Richter, R. Chang, B. Situ, Z. Chu, B. Burkemper, A. Reznik, S. Bedrood, A. H. Kashani, R. Varma, and R. K. Wang, "Diagnostic performance of macular versus peripapillary vessel parameters by optical coherence tomography angiography for glaucoma," *Translational Vision Science & Technology*, vol. 7, no. 6, pp. 21–21, 2018.
- [40] M. Alam, D. Thapa, J. I. Lim, D. Cao, and X. Yao, "Computer-aided classification of sickle cell retinopathy using quantitative features in optical coherence tomography angiography," *Biomedical Optics Express*, vol. 8, no. 9, pp. 4206–4216, 2017.